Coherence and Chaos in the Kuramoto-Velarde Equation

James M. Hyman and Basil Nicolaenko

I. INTRODUCTION

In the past decade, research into the behavior of finite dimensional dynamical systems has deepened our understanding of the transition to chaos in dissipative physical models. Underlying this explosive research field is the belief that transitions to chaos are generic, low-dimensional phenomena, even for continuum fluid flows governed by an infinite number of degrees of freedom. This is the essence of Feigenbaum's universality theory [19].

Yet, the fundamental problem remains open: are these transitions to dynamical chaos a route to fully developed turbulence in complex fluid flows [2-5, 9-11, 33-34]? A growing body of carefully controlled experiments suggests this is the case [7, 32], although when critical parameters such as the Reynolds number reach even moderate values, the physical detection of a small set of degrees of freedom is quickly blurred by statistical experimental noise [30].

Current computer calculations are unable to accurately simulate the full route to three-dimensional fluid turbulence. The next generation of supercomputers will have enough brute force to allow us to glimpse at the details of the transition to turbulence in the Navier-Stokes equations. Before they are available, we can study turbulent phenomena which can be modeled by one- and two-dimensional scalar partial differential equations (PDEs). In this paper, we

DIRECTIONS IN PARTIAL DIFFERENTIAL EQUATIONS

ISBN 0-12-195255-X

focus on PDEs that model localized patterns and structures appearing on interfaces between complex flows. They occur in quasi-planar flame fronts [4], thin viscous fluid films flowing over inclined planes, and the dendritic phase change fronts in binary alloy mixtures [31]. The solution of some of these models is indistinguishable from the solution of a finite-dimensional dynamical system.

In these models, as a critical physical parameter is varied, a simple laminar solution destabilizes. The destabilization is heralded by the cohesive organization of cells and patterns (often hexagonal) on the moving front or interface. The turbulence, localized on the interface, is dominated by fluctuations in the normal direction. As the critical parameter is increased, the spatial cells remain coherent, yet temporal behavior becomes chaotic. This behavior has been observed in flame-sheet experiments during the transition to fully turbulent flames [1]. The coexistence of spatial coherence with temporal chaos in these experiments makes them superb candidates for mathematical and computational testing of the link between deterministic chaos [19] and turbulence.

Many interfaces with localized turbulence, including flames, can be modeled by the simple Kuramoto-Sivashinsky (K-S) PDE [26-29, 31]. This equation accurately accounts for the thermodiffusive and convective mechanism of flow-field coupling across an interface before turbulence breaks away from the interface and reaches deeply into the fluid. In one space dimension, the K-S equation modeling a small perturbation $u(x,t)$ of a metastable planar front or interface is

$$\begin{aligned} &u_t + \nu u_{xxxx} + u_{xx} + \tfrac{1}{2}(u_x)^2 = 0 \quad , \quad (x,t) \in R^1 \times R_+ \quad , \\ &u(x,0) = u_o(x) \quad , \quad u(x + L) = u(x,t) \quad . \end{aligned} \tag{1.1}$$

Here the subscripts indicate partial differentiation, ν is a positive fourth-order viscosity, and u_o is L-periodic; L being the size of a typical pattern scale. The natural bifurcation parameter is the renormalized dimensionless

parameter $\tilde{L} = L/(2\pi\sqrt{\nu})$; $[\tilde{L}]$ is also the number of linearly unstable Fourier modes.

A related model is the Kuramoto-Velarde (K-V) equation [17]:

$$u_t + \nu u_{xxxx} + u_{xx} + \beta u + \gamma (u_x)^2 + \delta (u u_x)_x - \frac{\gamma}{L} \int_0^L (u_x)^2 \, dx = 0 \quad , \qquad (1.2)$$

$$\int_0^L u(x,t) \, dx \equiv 0 \quad ,$$

where β, γ, δ are positive, $\beta << 1$, and with periodic boundary conditions and initial conditions with zero mean. The K-V equation models Benard-Marangoni cells that occur when there is large surface tension on the interface [35, 36] in a microgravity environment [16, 17]. This situation arises in crystal growth experiments aboard an orbiting space station. Although the free interface is metastable with respect to small perturbations, the nonlinearity $\delta(uu_x)_x$, not present in the K-S equation, models pressure destabilization effects striving to rupture the interface.

Our computer simulations of the K-S equation [24] demonstrated an uncanny intermittent, low-dimensional behavior for the values of the bifurcation parameter beyond the point where the transition to chaos had occurred. Some canonical mechanisms for onset of chaos [19] in classical dynamical systems are seen amidst complex and lengthy turbulent time series. In this article, we report on a similar systematic study of the transition to chaos for the K-V equation.

If the eikonal nonlinearity term u_x^2 in (1.2) is removed ($\gamma = 0$, $\beta \geq 0$), then the solution of the K-V equation and its gradients blow up in finite time. We have verified this numerically and demonstrated it using classical methods [Ladyshenskaia]. Furthermore, in our numerical studies we found that the convective term u_x^2 not only controls blowup in (2.6), but also generates chaotic dynamics qualitatively similar to those of K-S. In this paper we systematically search for classical dynamical systems bifurcations and for

multiple basins of attractions for the K-V model. As in the K-S model [24], we have uncovered a rich solution structure with multiple internal attractors having interlaced basins of attraction.

When we solve chaotic PDEs, the reliability of the long-term, time-dependent behavior is always in question until a comprehensive error analysis is performed. In our computer experiments, we found that the calculated solutions could be extremely sensitive to the numerical accuracy. Nonconverged numerical solutions of the K-S and K-V equations can occur in regimes we are interested in if the time integration errors are greater than 10^{-6} per unit timestep. In fact, small effects of the order of 10^{-6} in the energy for some sensitive Fourier modes can critically impact on the nonlinear dynamics. In the calculations, we used discrete Fourier transform pseudospectral approximations to the spatial derivatives [22] on grids ranging from 64 to 256 mesh points in single precision (14 digits) on a Cray XMP computer. The solution was integrated in time using a variable order, variable timestep backward differentiation method [21] that retained an absolute error tolerance between 10^{-6} and 10^{-10} per unit time. The runs presented here took between 10^4 and 10^5 time-steps. The implicit equation was solved on each timestep with a quasi-Newton iterative algorithm. Because these equations were not solved exactly, a symmetry-breaking perturbation was introduced into the calculation. Many of the current calculations use an approximate solution operator (ASO) based on finite Fourier transforms and an exponential trapezoidal rule [23]. The ASO methodology incorporates analytic information on the behavior of the solution into the numerical approximation.

A typical example of the extreme numerical sensitivity of the numerical solutions to the K-S and K-V equations is the disappearance of homoclinic orbits if the precision is too low. The saddle-type hyperbolic fixed points degenerate into numerically stable fixed points with an artificial basin of attraction the size of the error control. Because of the artificially stable fixed points, our numerical results of

the K-S and K-V equations differ from some of the previously published simulations with only modest control over time integration errors.

II. OVERVIEW OF COMPUTATIONAL SIMULATIONS AND THEORETICAL RESULTS

In our calculations, we normalized the K-S equation to an interval of length 2π, set the damping parameter to the original value derived by Sivashinsky ($\nu = 4$), and introduced the bifurcation parameter $\alpha = 4\tilde{L}^2 = L^2/4\pi^2$:

$$u_t + 4u_{xxxx} + \alpha\,[u_{xx} + \tfrac{1}{2}(u_x)^2] = 0 \quad , \quad 0 \le x \le 2\pi \quad , \tag{2.1}$$

$$u(x + 2\pi, t) = u(x,t) \quad , \quad u(x,0) = u_o(x) \quad .$$

This equation is equivalent to Eq. (1.1) with a different time scaling.

The mean value of the solution to Eq. (2.1)

$$m(t) = \frac{1}{2\pi} \int_0^{2\pi} u(x,t)dx \tag{2.2}$$

satisfies the drift equation

$$\dot{m}(t) = \frac{-\alpha}{4\pi} \int_0^{2\pi} (u_x)^2 \, dx \quad . \tag{2.3}$$

To normalize this drift to zero, we numerically solved the drift-free K-S equation for

$$v(x,t) = u(x,t) - m(t) \quad . \tag{2.4}$$

That is,

$$v_t + 4v_{xxxx} + \alpha[v_{xx} + \tfrac{1}{2}(v_x)^2] + \dot{m}(t) = 0 \quad . \tag{2.5}$$

We also normalized the K-V equation on $[0,2\pi]$ and set $\nu = 4$, $\gamma = \tfrac{1}{2}$, $\delta = 1$ (comparable nonlinearities). In most situations $\beta << 1$ and, therefore, for simplicity and to allow a systematic comparison with the K-S [24], we consider the

case $\beta \equiv 0$ and define $\alpha = L^2/4\pi^2$. The drift-free K-V equation is then

$$u_t + 4u_{xxxx} + \alpha[u_{xx} + \tfrac{1}{2}(u_x)^2 + (uu_x)_x]$$

$$- \frac{\alpha}{4\pi} \int_0^{2\pi} (u_x)^2 \, dx = 0 \quad , \quad 0 \le x \le 2\pi \quad , \qquad (2.6)$$

$$u(x + 2\pi, t) = u(x,t) \quad , \quad u(x,0) = u_o(x) \quad .$$

We consider only initial values with zero mean. This implies that there is no cavitation and that the liquid follows the interfacial motion [16, 17].

The computational explorations outlined in [24] and here have spurred efforts to prove that the K-S and K-V equations are rigorously equivalent to a finite dynamical system. The approach (introduced in [12-15]) consists of constructing a finite dimensional Lifschitz inertial manifold Σ in the phase space of the PDE such that

(i) Σ is invariant and has compact support; that is, if $(S(t,\cdot))_{t\ge 0}$ is the nonlinear semigroup associated with the initial value problem for the equations, then $S(t,\Sigma)$ is contained in Σ for all $t \ge 0$.

(ii) All solutions converge exponentially to Σ. In particular, the universal attractor, X, is included in Σ and the dissipative PDE reduces on Σ to a finite dynamical system (called an inertial ODE). More details of this structure can be found in the paper by C. Foias, in these proceedings.

The existence of such an inertial manifold has been demonstrated [6, 14, 15, 29] for the K-S equation with Neumann boundary condition. In this case the dimension of Σ is less than $c\alpha^{1.75}$, where c is a constant independent of α. This can be compared with an upper bound for the fractal dimension of the universal attractor X [28], $d_f(X) \le c\alpha^{0.75}$). It has been proven that all solutions of (1.1) with Neumann boundary conditions converge exponentially, as $O(\exp -c\alpha^5 t)$, to the inertial manifold Σ. Thus when $\alpha > 1$, the solution is practically on the inertial manifold almost immediately. This is the essence of the argument that the K-S equation

is a paradigm of a PDE equivalent to a finite dynamical system. Similar results hold for the K-V equation [Nicolaenko, unpublished] and for a model of 2-D weak turbulence in shear flows [8].

The bifurcation catalogues and diagrams (Figs. 1 and 2), were created by systematically scanning large intervals in the bifurcation parameter α. The diagrams for the K-S equation (Figs. 1b and 2b) are described elsewhere in detail [24]. While keeping α fixed, we searched for different attractors by varying the initial conditions. We then tracked the domains of stability of each attractor with respect to the bifurcation parameter by varying α and reinitializing $v(x,0)$ to the final solution from the previous run with a different α. Many problems were recalculated several times with different grid resolutions and time truncation error criteria to ensure that the numerical solutions were converged within an acceptable accuracy.

A remarkable feature of both the K-S and K-V equations is the alternating sequence of intervals in α that contain either laminar behavior, where a fixed point is ultimately attracting, or persistent oscillatory and/or chaotic behavior. Let $I_j = [\alpha_j, \alpha_{j+1}]$ be the j^{th} interval. If α_1 is the point where the first Hopf bifurcation occurs, then $I_0 = [0, \alpha_1]$. A static pitchfork-like steady-state bifurcation occurs at $\alpha = 4 < \alpha_1$ for the K-V equation (Fig. 1a). For j <u>even</u>, I_j is characterized by the ultimate decay to a globally attracting fixed point $\tilde{u}_q(x)$, $q = (j/2) + 1$, $j \geq 2$. These fixed points have most of their energy concentrated in the q-th mode. The higher harmonics appear with exponentially decreasing energy and the fixed point has a lacunary Fourier expansion:

$$\tilde{u}_q(x) = a_{1q} \cos qx + \varepsilon\, a_{2q} \cos 2qx + \varepsilon^2\, a_{3q} \cos 3qx + \ldots + \varepsilon^{n-1}\, a_{nq} \cos nqx + \ldots \quad , \tag{2.7}$$

where $q = j/2+1$. Numerically, we have found that a_{1q} is O(1) and $\varepsilon \cong 10^{-1}$. We call these sinks associated with I_j, j even, <u>cellular states</u>. When the Fourier expansion (2.7) of a

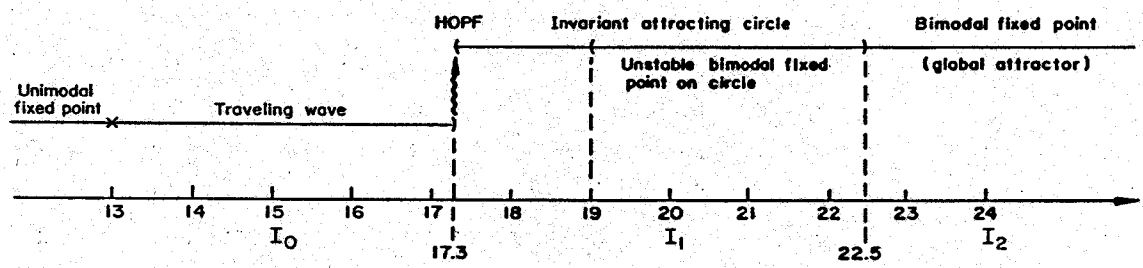

Fig. 1a. Stable solution of the K-S equation.

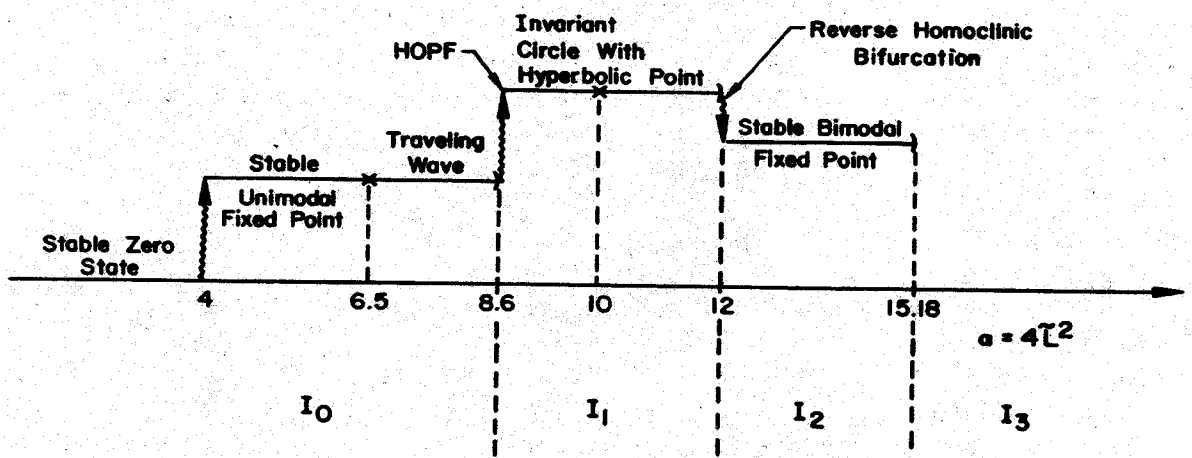

Fig. 1b. Stable solutions of the K-V equation.

Fig. 1. The stable solution manifolds for the K-S (Fig. 1a) and K-V (Fig. 1b) equation have a simple structure when α is small.

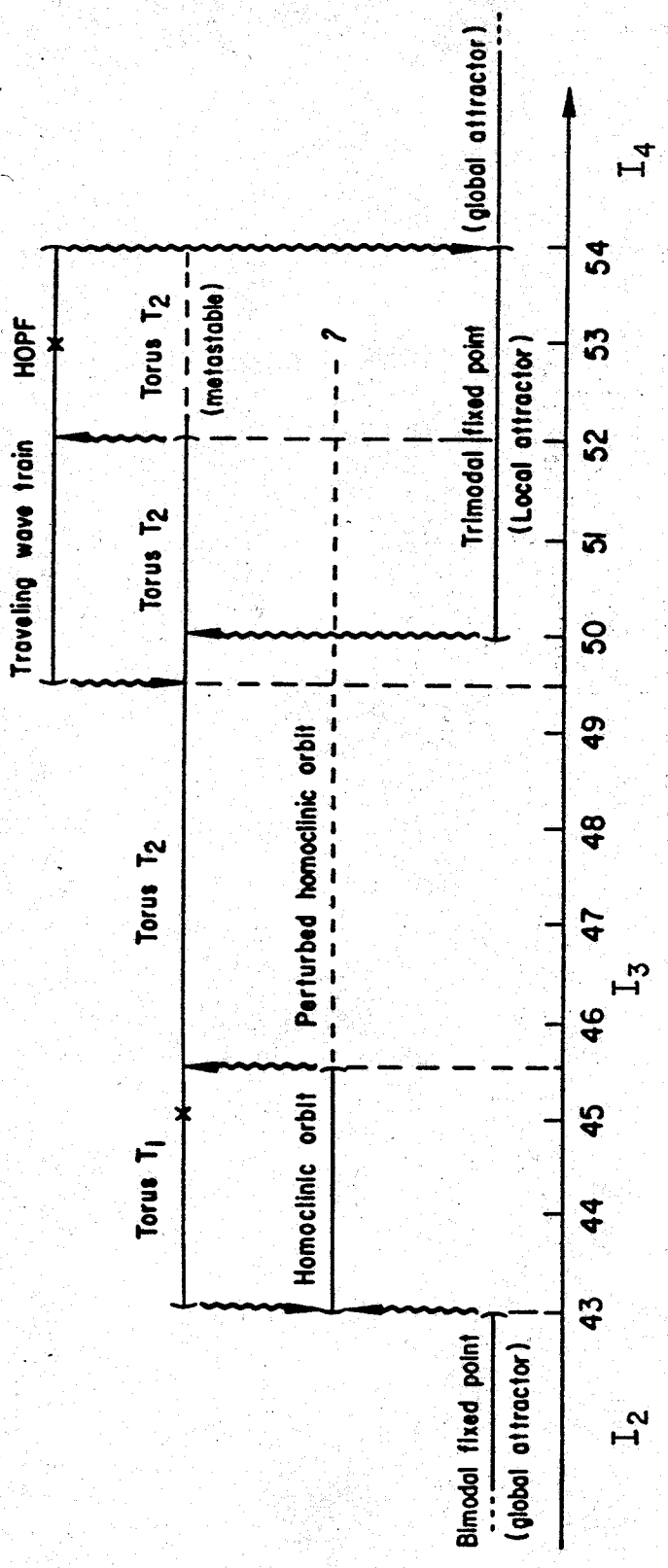

Fig. 2a. As the bifurcation parameter increases, the stable solution manifolds of the K-S equation become more complex.

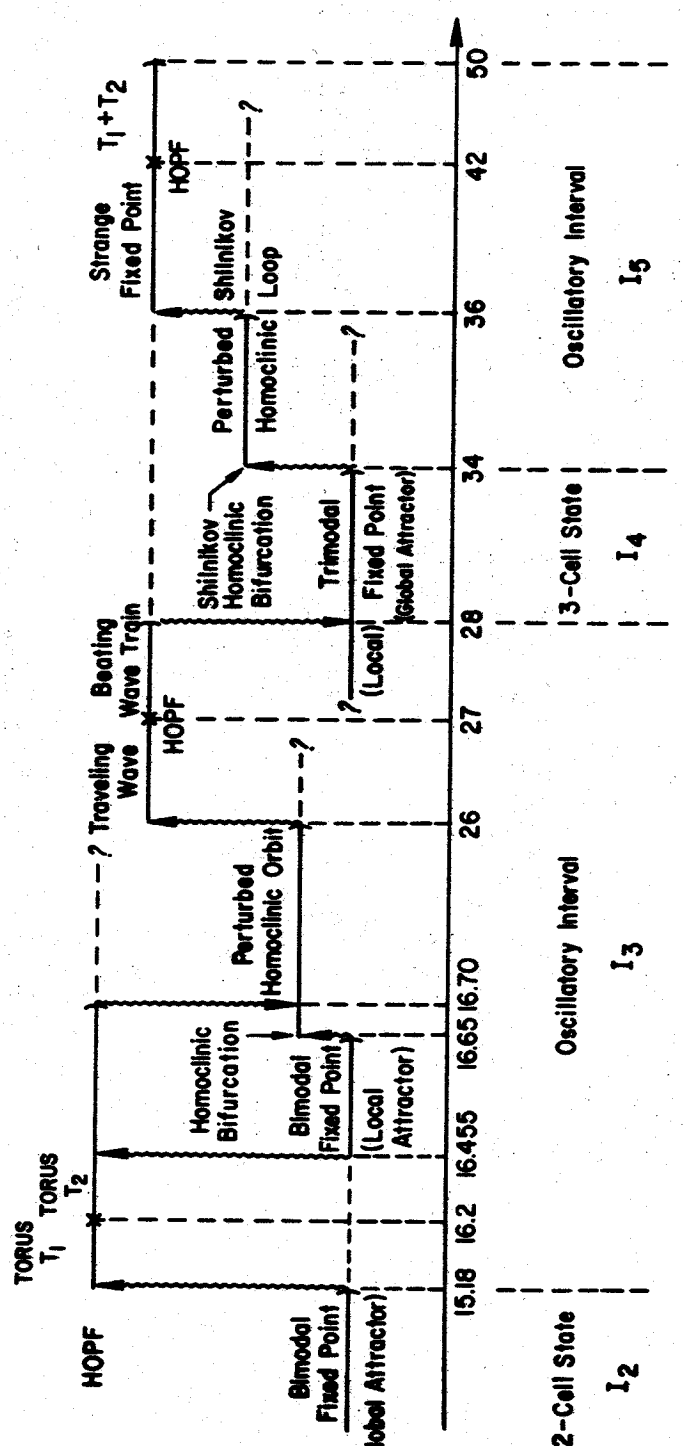

Fig. 2b. As the bifurcation parameter increases, the stable solution manifolds of the K-V equation become more complex.

cellular state is dominated by the q-th mode, we call it a q-modal cellular state.

The relaminarization intervals I_j, j even, are consistent with experiments at small and moderate Reynolds numbers [32]. Moreover, as j and α increase, the ultimate decay follows long periods of transient chaos. Transient chaos is observed in both the K-S and K-V equations beginning at the interval I_4, provided enough modes are excited in the initial data. Moreover, as α increases, the mean lifetime of transient chaos increases exponentially in $\tilde{L}$. When the fractal dimension of the universal attractor, X, for the flow is large, $\dim_f(X) \geq 10$, this growth makes transient chaotic intervals undistinguishable, in practice, from chaotic intervals in the strongly chaotic regimes.

When j is odd, the intervals I_j have persistent oscillatory and/or chaotic behavior. For moderate values of α (up to about I_7), the quasi-periodic and/or chaotic behavior reflects a competition between the previous j+1/2 cellular state and the j+3/2 cellular state. This competition creates a complex interplay between temporal chaos and spatial coherence. In some sense, the (low-dimensional) temporal chaos in I_j corresponds to adjustment from one (low-dimensional) space pattern to the next one.

III. THE K-V EQUATION BIFURCATION INTERVALS

In this section, we describe the behavior of the solutions to the K-V equation for parameter values in the intervals I_j, $0 \leq j \leq 5$, $0 \leq \alpha \leq 50$ ($0 \leq \tilde{L} \leq 3.53$). Within these intervals we see canonical vector field bifurcations leading to quasi-periodic motion and chaos. By systematically varying the initial conditions and α, we have constructed the preliminary bifurcation catalogue of the attractors to Eq. (2.6) shown in Figs. 1b and 2b.

These windows (intervals I_j) are much narrower than the corresponding ones for the K-S equation (Figs. 1a and 2a). Indeed, at $\alpha = 50$, we are still in the quasi-periodic window I_3 for the K-S equation, but K-V has reached the end of the oscillatory window I_5. The term $(u_x)^2$ controls the blowup, but the nonlinearity $(uu_x)_x$ in the K-V equation accelerates

the transition to chaos. Within each window, the bifurcation sequences for the K-S and K-V equations are generically similar: homoclinic loops, perturbed transverse homoclinic orbits and low-dimensional tori which eventually break up. In addition, here is a wealth of reverse bifurcations attractors that alternatively destabilize and restabilize again at some larger α.

In the discussion below, the "energy" is the integral of $(u_x)^2$ and the "energy in mode k" is the modulus of the k^{th} Fourier coefficient.

The first bifurcation in the K-V equation is a classical pitchfork bifurcation at $\alpha = 4$ ($\tilde{L} = 1$) into a unimodal cellular state. At $\alpha = 6.50$, it bifurcates into a traveling wave (a similar phenomenon occurs in K-S at $\alpha = 13.0$). At $\alpha = 8.60$, the traveling unimodal wave undergoes Hopf bifurcation into an invariant circle. Surprisingly, this first sequence does not lead to further bifurcations and transition to chaos. The invariant circle remains attracting, yet a hyperbolic bimodal cellular point (repelling) is evident near $\alpha \cong 10$. At $\alpha = 12$ it undergoes a reverse homoclinic bifurcation [20] and the window I_1, $8.60 \leq \alpha \leq 12$, ends. In the interval I_2, $12 < \alpha < 15.18$, the bimodal fixed point, $\tilde{u}_2(x,\alpha)$, is globally attracting.

The second oscillatory window I_3 begins at $\alpha = 15.18$ where $\tilde{u}_2$ undergoes a nonclassical Hopf bifurcation that breaks the symmetry [18]. That is, the bifurcated circle breaks the group invariance $u(x,t) \to u(-x,t)$ of K-V. Tracking this torus T_1 (circle) by numerical continuation, we observed its bifurcation into T_2 (a two-dimensional torus) near $\alpha \cong 16.20$, with quasi-periodic dynamics (two incommensurate frequencies). This T_2 becomes metastable at $\alpha = 16.70$.

The attractor $T_1 + T_2$ is globally attracting for $15.18 \leq \alpha < 16.455$, but has only a limited basin of attraction for $16.455 \leq \alpha < 16.70$. At $\alpha = 16.455$, the bimodal cellular state $\tilde{u}_2$ undergoes its second reverse bifurcation and becomes a sink. It has a small basin of attraction on $16.455 < \alpha < 16.65$ where

$$\tilde{u}_2 = 5.9\cos 2x + 0.98\cos 4x + 0.09\cos 6x + \ldots \qquad (3.1)$$

(at $\alpha = 16.455$) is stable with respect to small perturbations. The interval $16.455 \leq \alpha \leq 16.70$ is the first occurrence of coexisting attractors.

At $\alpha = 16.65$, a homoclinic loop appears with an infinite period orbit as $\tilde{u}_2$ undergoes its second (direct) homoclinic bifurcation [19]. As α increases, $\tilde{u}_2$ remains hyperbolic, with a nearly periodic, perturbed homoclinic orbit. The numerical example in Fig. 3 illustrates this for $\alpha = 22$, $u_0(x) = 6\cos 2x + \cos 4x$. The solution orbit spends a substantial time in a neighborhood of the saddle point

$$\tilde{u}_2(x) = 4.5\cos 2x + 1.15\cos 4x + 0.125\cos 6x + \ldots \quad . \qquad (3.2)$$

The motion around the loop is triggered by a sensitive nonlinear exchange of energy between the odd and even modes. In Fig. 3b, the energy in Mode 1 bursts quickly from 10^{-7} to 10 as the solution traverses around the (perturbed) homoclinic loop. A corresponding dip is observed in the energy of Mode 2 (Fig. 3c).

These calculations were done with an error tolerance of 10^{-8} per unit timestep. When we relaxed the precision of the numerical integrations above 10^{-6}, the homoclinic loop disappeared and the solution locked into the numerically attracting bimodal fixed point. The high precision was necessary to trigger the energy feedback into the odd modes. Additional calculations with an error tolerance of 10^{-10} comfirmed that the homoclinic loop was not an artifact. This is one example (among many) that alerted us to the extreme sensitivity of the oscillatory solutions to the precision of the numerical method.

Similar dynamics associated with the stable and unstable manifolds of $\tilde{u}_2$ are observed until $\alpha \cong 26$, where a stable traveling wave train appears as a global attractor. This wave train is not related to either the previous bimodal point or to the trimodal cellular state, which is a global sink in I_4. It seems to be a special orbit on the metastable

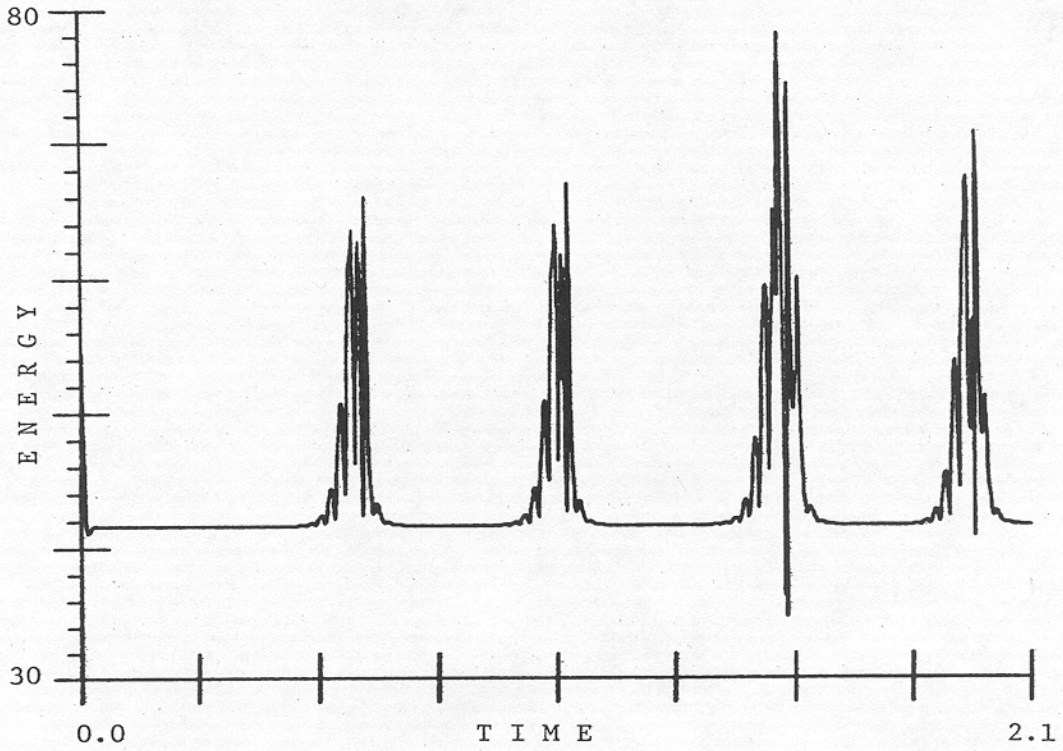

Fig. 3a. The energy of the solution has periodic bursts on the homoclinic loop (K-V, α = 27).

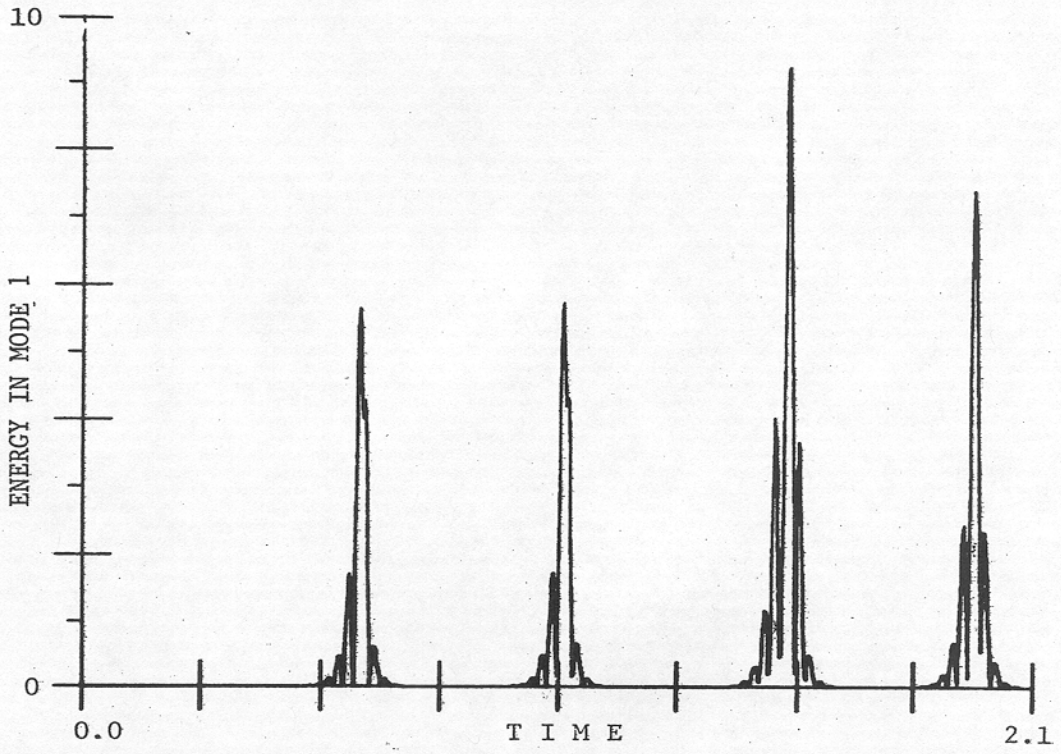

Fig. 3b. The energy in the first mode decays almost to zero near the bimodal saddle point.

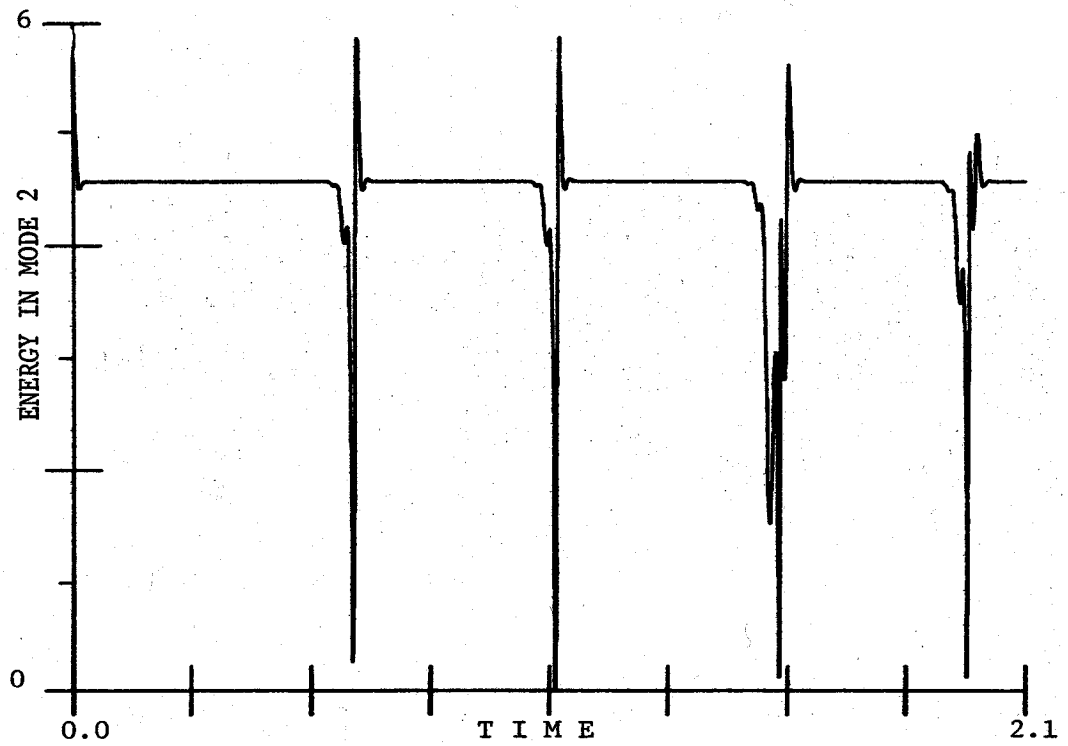

Fig. 3c. The energy in the second mode is nearly constant between the bursts. The saddle point has energy only in the even modes.

torus T_2. Its Fourier series expansion is not lacunary and a typical profile has two humps, a large one and a small one.

At $\alpha = 27$, the wave train undergoes Hopf bifurcation and becomes a strongly beating wave. The oscillations in the energy of the beating wave are evident in Fig. 4a ($\alpha = 27$, $u_0(x) = \cos x + \sin x + \cos 2x + \sin 2x + \cos 3x + \sin 3x + \cos 4x + \sin 4x$). The contour levels of the solution in Fig. 4b show the beating wave train drifting alternatively from left to right.

The window I_3 ends at $\alpha = 28$, where the trimodal cellular state

$$\tilde{u}_3 = 5.9 \cos 3x + 0.8 \cos 6x + \ldots \qquad (3.3)$$

becomes a global sink. At $\alpha = 28$, initial conditions were imposed in which the first six cosine and sine modes were excited to a level of O(1); the solution displayed persistent

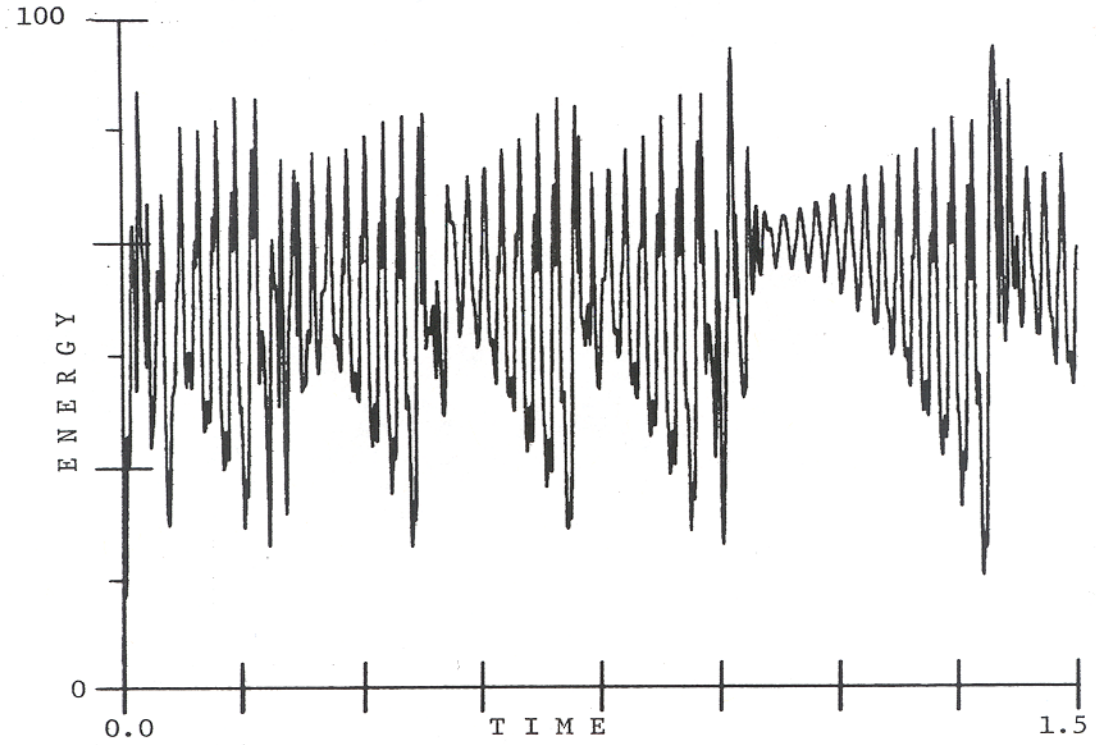

Fig. 4a. The traveling wave undergoes a Hopf bifurcation at $\alpha = 27$ (K-V) into a beating wave train.

Fig. 4b. The contour plot of the beating wave solution shows it drifting in alternate directions.

near-chaotic behavior before crashing abruptly into $\tilde{u}_3$. This type of transient behavior at the onset of an even-numbered interval heralds the transient chaos observed for large α's. The window I_4 spans $28 < \alpha < 34$.

These solutions linger in the background at higher α. The two-humped structure observed for $26 \leq \alpha \leq 27$ reoccurs in the midst of the next oscillatory interval I_5 (see Fig. 2b). At $\alpha = 36$, a steady, nondrifting, nonbeating fixed point reappears as a global attractor, with a similar two-humped profile (see Fig. 5). This strange fixed point has substantial energy in the first six modes and persists as a global sink until $\alpha = 42$, where it undergoes another Hopf bifurcation. The new Torus T_1 quickly evolves into T_2 and breaks down into near-chaotic dynamics. The transition into I_6 ($\tilde{u}_4$) occurs near $\alpha \cong 50$.

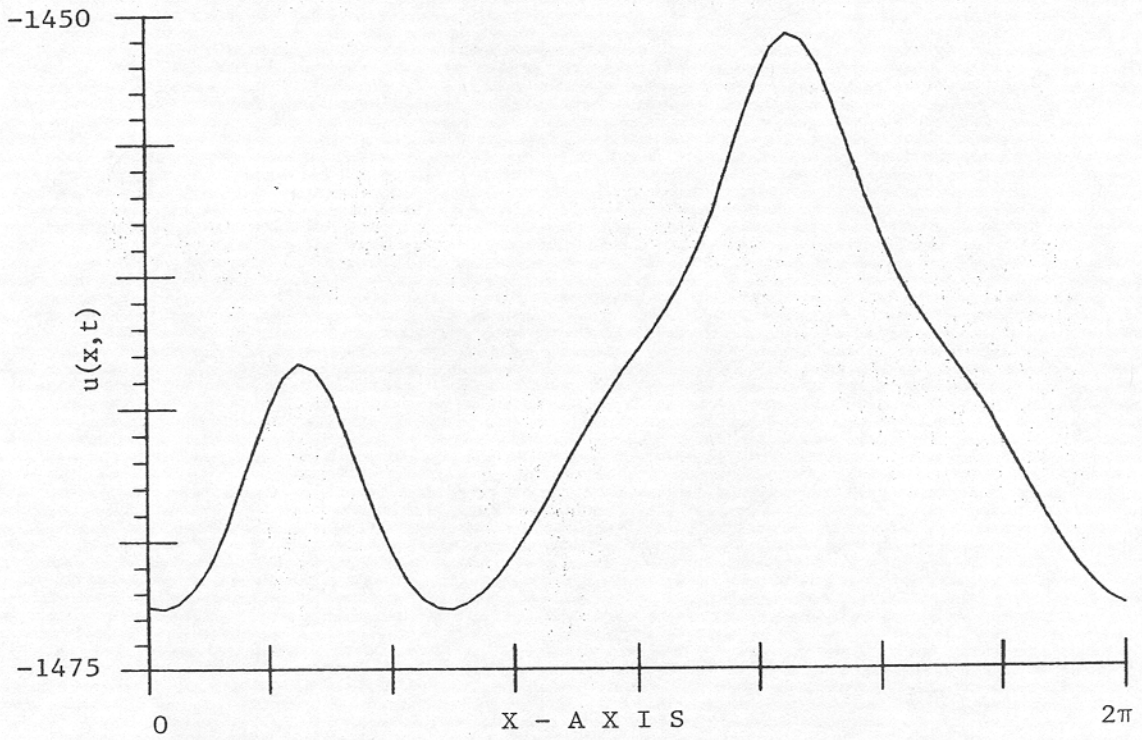

Fig. 5. This two-humped fixed point appears at $\alpha = 36$. Glimpses of it also appear in the traveling and beating waves at $26 < \alpha < 28$.

At $\alpha = 34$, the trimodal cellular state $\tilde{u}_3$ (a global sink in I_4) bifurcates. The bifurcation is neither of Hopf type, nor through a classical homoclinic loop. This is explored in Fig. 6 ($\alpha = 34$, $u_0 = 6\cos 3x + 0.8\cos 6x + 0.1\sin x$). At roughly periodic intervals, the orbit bursts away on the unstable manifold of $\tilde{u}_3$, intermittently puffs into chaos at a much lower energy level, and then spirals back around the hyperbolic point $\tilde{u}_3$. Fig. 6b confirms that the energy in the first mode is low during the small oscillations around the spiral hyperbolic point $\tilde{u}_3$ and is much higher during the chaotic bursts. The energy in the third mode, Fig. 6c, is the mirror image of Fig. 6b. It oscillates in a small neighborhood of 5.9, then bursts away from $\tilde{u}_3$ into a chaotic excursion. This behavior persists until $\alpha = 36$ and has many of the characteristics of a perturbed Shilnikov homoclinic loop [19] associated with a spiral hyperbolic point. To our knowledge, this is the first time it has been observed in a parabolic PDE. This behavior has also been observed and proved to exist for traveling wave solutions of the Fitz Hugh-Nagumo equation [25].

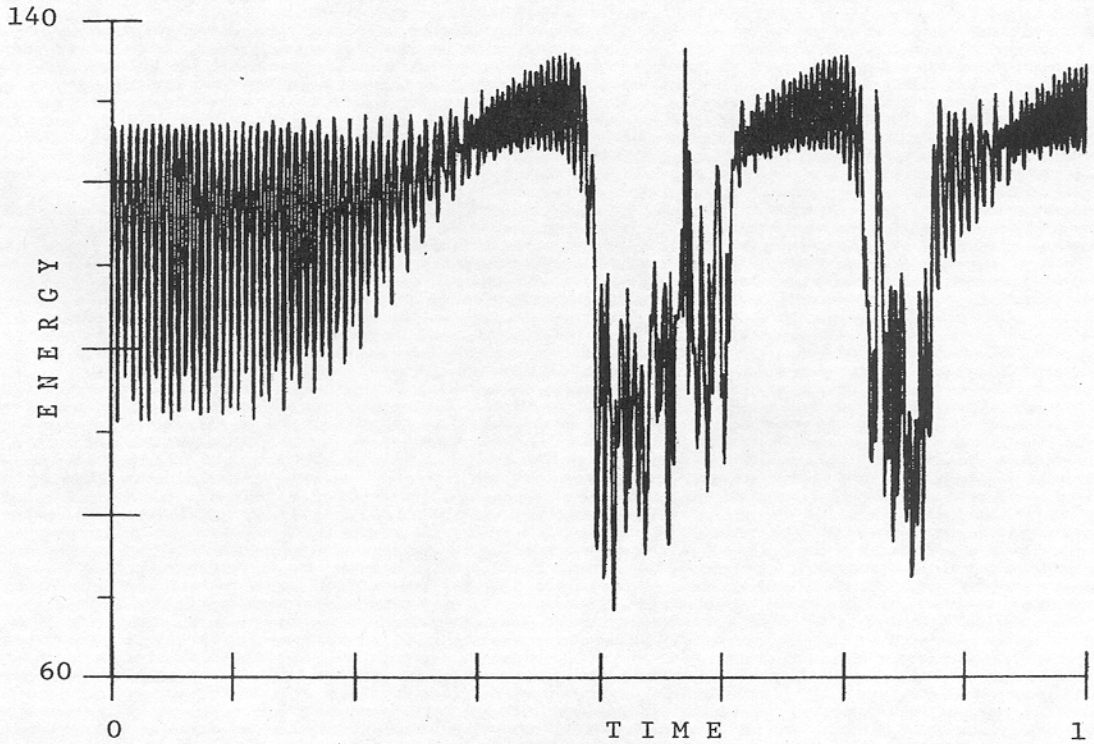

Fig. 6a. The energy has near-periodic bursts on the homoclinic loop and then spirals around the hyperbolic point (Shilnikov homoclinic loop, $\alpha = 34$, K-V).

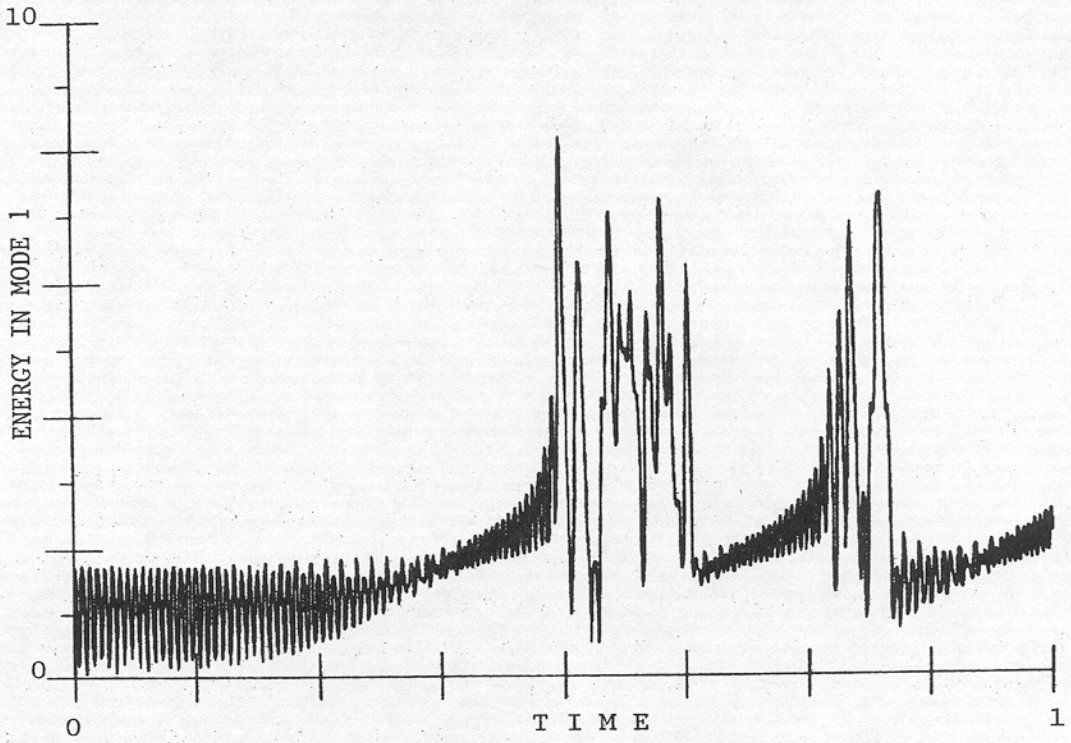

Fig. 6b. The energy in the first mode is low during the small oscillations near the trimodal hyperbolic point.

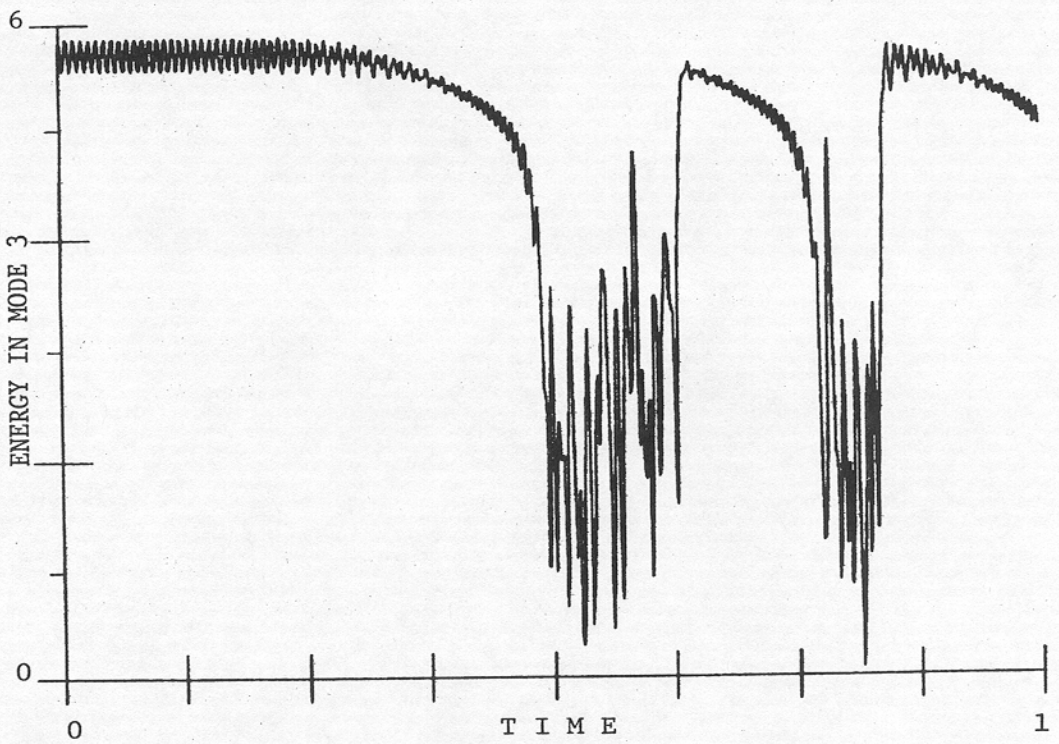

Fig. 6c. The energy in the third mode is high in the neighborhood of the spiral hyperbolic point, whose components contain energy only in the harmonics of three.

The bifurcations of the K-V equation, unraveled in this section, occur on low-dimensional inertial manifolds. Multiple forward and reverse bifurcations of several cellular fixed points are entangled in a web of tori, together with hyperbolic points. For these regimes, we conjecture that it may be possible to construct a simple reduced inertial normal form for the ODEs on the inertial manifold using the unstable manifolds of $\tilde{u}_2(x,\alpha)$, $\tilde{u}_3(x,\alpha)$, and the two-humped strange fixed point (Fig. 5).

IV. SUMMARY

A low-dimensional vector field skeleton underpins the sometimes chaotic solutions of the K-S and K-V turbulent interface models. This low-dimensional subtle architecture is mirrored by repeated bifurcations and intermittencies in the solution dynamics and plays a crucial role in bridging the gap between strong dynamical chaos and fully developed turbulence. Current analytic results [6] support the numerical evidence that this small exotic zoo of hyperbolic points and tori generates strong chaos in the K-S and K-V equations. We suspect that the dynamically relevant strange fixed points will be embedded in a Cantor-like structure in space (this has been proved for K-S, $\alpha = \infty$, by D. M. Michelson) and that spatial chaos will intermingle with temporal chaos at large values of the bifurcation parameter.

ACKNOWLEDGMENTS

The authors thank I. Kevrekidis for his helpful discussions and J. L. Castillo, P. L. Garcia-Ybarra, and M. G. Velarde for suggesting computational explorations of their model.

REFERENCES

1. P. Clavin, "Dynamic Behavior of Premixed Flame Fronts in Laminar and Turbulent Flows," Prog. Energy. Combust. Sci. 11 (1985), 1-59.
2. P. Constantine and C. Foias, Comm. Pure Appl. Math. 38 (1985), 1-27.

3. P. Constantine, C. Foias and R. Temam, Memoirs AMS 53 (1985) #314, vii+.67pp.
4. P. Constantine, C. Foias, O. P. Manley and R. Temam, C. R. Acad. Sci. Paris I, 297 (1983) 599-602.
5. P. Constantine, C. Foias, O. P. Manley and R. Temam, J. Fluid Mech. 150 (1985) 427-440.
6. P. Constantine, C. Foias, B. Nicolaenko and R. Temam, "Integral Manifolds and Inertial Manifolds for Dissipative PDE's (submitted).
7. J. D. Farmer, E. Jen, A. Brandstäter, J. Swift, H. L. Swinney, A. Wolff and J. P. Crutchfield, "Low Dimensional Chaos in a Hydrodynamic System," Phys. Rev. Lett. 51, 16 (1983) 1442-1445. See also J. P. Gollub and H. L. Swinney, Phys. Rev. Lett. 35 (1975) 927.
8. C. Foias, B. Nicolaenko and R. Temam, "Asymptotic Study of an Equation of G. I. Sivashinksy for Two Dimensional Turbulence of the Kolmogorov Flow," to appear, Proc. Paris Acad. Sci.
9. C. Foias and R. Temam, C. R. Acad. Sci. Paris, I, 295 (1982) 239-241.
10. C. Foias and R. Temam, C. R. Acad. Sci. Paris, I, 295 (1982) 523-525.
11. C. Foias and R. Temam, Mathematics of Computation 43 (1984) 117-133.
12. C. Foias, G. R. Sell and R. Temam, C. R. Acad. Sci. Paris, I, 301 (1985) 139-141.
13. C. Foias, G. R. Sell and R. Temam, "Inertial Manifolds for Dissipative PDE's (submitted).
14. C. Foias, B. Nicolaenko, G. R. Sell and R. Temam, C. R. Acad. Sci. Paris, I, 301 (1985) 285-288.
15. C. Foias, B. Nicolaenko, G. R. Sell and R. Temam, "Inertial Manifolds and an Estimate of Their Dimension for the Kuramoto-Sivashinsky Equation (submitted).
16. P. L. Garcia-Ybarra and M. G. Velarde, "Oscillatory Marangoni-Benard Interfacial Instability and Capillary-Gravity Waves in Single and Two-Component Liquid Layers with or without Soret Thermal Diffusion," to appear.
17. P. L. Garcia-Ybarra, J. L. Castillo and M. G. Velarde, "Benard-Marangoni Convection with a Deformable Interface and Poorly Conducting Boundaries," to appear.

18. M. Golubitsky and D. G. Schaeffer, "Singularities and Groups in Bifurcation Theory," Springer-Verlag, New York 1985).
19. J. Guckenheimer and P. H. Holmes, Nonlinear Oscillations, Dynamical Systems and Bifurcation of Vector Fields, Springer-Verlag (1985).
20. J. Guckenheimer, "Strange Attractors in Fluids: Another View," Annual Review of Fluid Mechanics (1986).
21. J. M. Hyman, "MOLID: A General Purpose Subroutine Package for the Numerical Solution of Partial Differential Equations," Los Alamos Scientific Laboratory Manual, LA-7595-M (1978).
22. J. M. Hyman, "Numerical Methods for Nonlinear Differential Equations," Nonlinear Problems: Present and Future, A. R. Bishop, D. K. Campbell and B. Nicolaenko, Eds., North-Holland Publ. Co., (1982) 91-107.
23. J. M. Hyman, "Numerical Methods Based on Analytic Approximations" (in preparation).
24. J. M. Hyman and B. Nicolaenko, "The Kuramoto-Sivashinsky Equation: a Bridge Between PDE's and Dynamical Systems," to appear in Physica D (1986).
25. Guan-Hsong Hsu, Ph.D. Thesis, 1985, Courant Institute of Math. Sciences, New York University.
26. B. Nicolaenko and B. Scheurer, "Remarks on the Kuramoto-Sivashinsky Equation," Physica 12D (1984) 331-395.
27. B. Nicolaenko, B. Scheurer, and R. Temam, "Quelques proprietes des attracteurs pourl'equation de Kuramoto-Sivashinsky," C. R. Acad Sci. Paris 298 (1984) 23-25.
28. B. Nicolaenko, B. Scheurer, and R. Temam, "Attractors for the Kuramoto-Sivashinsky Equations," Physica 16D (1985) 155-183.
29. B. Nicolaenko, B. Scheurer, and R. Temam, "Attractors for the Kuramoto-Sivashinsky Equations," AMS-SIAM Lectures in Applied Mathematics 23, 2 (1986) 149-170.
30. B. Nicolaenko, B. Scheurer, and R. Temam, "Attractors for Classes of Nonlinear Evolution of Partial Differential Equations," in preparation.

31. G. I. Sivashinsky and A. Novick-Cohen, "Interfacial Instabilities in Dilute Binary Mixtures Change of Phase, to appear in Physica D.
32. K. Shreenivasan, "Transition and Turbulence in Fluid Flows and Low-Dimensional Chaos," Frontiers in Fluid Mechanics, S. H. Davis and J. L. Lumley, Eds., Springer-Verlag (1985) 41-67.
33. R. Temam, Navier Stokes Equations and Nonlinear Functional Analysis, SIAM, Philadelphia, 1983.
34. R. Temam, "Infinite Dimensional Dynamical Systems of Fluid Mechanics," AMS-Summer Res. Institute "Nonlinear Funct. Anal. Appl." (Berkeley, 1983).
35. M. G. Velarde and C. Normand, Sci. Amer. 243 (1980) 92.
36. M. G. Velarde and J. L. Castillo, "Convective Transport and Instability Phenomena, J. Zierep and H. Oertel, Jr., Eds., Braun-Verlag, Karlsruhe (1982).

The authors were supported by the US Department of Energy under contract W-7405-ENG-36 and the Office of Scientific Computing under contract KC-07-01-01-0.

Center for Nonlinear Studies
Theoretical Division, MS B284
Los Alamos National Laboratory
Los Alamos, NM 87545